THE ROLE OF THERMAL STRESS IN ENHANCING THE RESERVOIR PROPERTIES OF ENHANCED GEOTHERMAL

Musa D Aliyu[1], Rosalind A Archer[1]

[1]Department of Engineering Science, the University of Auckland, Private Bag 92019, Auckland 1142, New Zealand.

musa.aliyu@auckland.ac.nz

r.archer@auckland.ac.nz

Keywords: *Induced thermal stress, thermal shock, EGS reservoir, multifracture, horizontal wellbores.*

ABSTRACT

The injection of cold fluid into a hot dry rock (HDR) formation causes temperature changes that often induce thermal stress. This will alter the reservoir properties of the rock mass and the fluid, making thermal stress central to understanding the behaviour of HDR geothermal reservoirs. In order to explore the effect of thermal stress on reservoir properties, this paper presents a new numerical model of an enhanced geothermal system (EGS) using a coupled thermo-hydro-mechanical (THM) model. Nine reservoir properties are examined: permeability, aperture, stiffness, pore pressure, effective stress, shear stress, density, viscosity, and temperature. The results show that thermal stress enhances each of these properties substantially when compared with a model without thermal stress. It is clear from the simulation that exclusion of the thermal stress effect in a model could end in an erroneous description of the system output.

1. INTRODUCTION

Numerical modelling of enhanced geothermal system (EGS) reservoirs as a field of research dates back to 1972 (Abé et al., 1985, 1979, 1976b, 1976a; Abé and Sekine, 1983). Over these 50 years, extensive efforts have been made towards developing coupled thermo-hydro-mechanical (THM) models of EGS reservoirs (Al Saedi et al., 2019; M.D. Aliyu and Chen, 2017; Elsworth, 1989; Hicks et al., 1996; Tsang, 1999; Willis-Richards and Wallroth, 1995; Zimmerman, 2000). Harlow and Pracht (1972) pioneered the research in the field, solving the coupled processes of heat transport, fluid flow and rock fracture in hot dry rock (HDR) reservoirs using the finite difference (FD) scheme. The model considers the effects of fracture propagation on HDR exploitation. McFarland (1975) developed an FD model to describe the behaviour of an HDR geothermal reservoir with a vertically oriented crack created by hydraulic fracturing. Bažant and Ohtsubo (1978) employed McFarland's geometry to develop a finite element (FE) model of an HDR heat extraction scheme using the coupled processes of fluid flow, heat transport and rock fracture.

In the 1990s, several models were developed using field measurements or established computer codes to understand the long-term performance of HDR reservoirs. For example, Jupe et al. (1995) developed a coupled THM model of the European HDR project located at Soultz, France, to assess the minimum wellbore spacing required during circulation to meet the thermal performance objectives. Willis-Richards et al. (1996) described and applied a two-dimensional (2D) coupled THM network model of hydraulic stimulation for three HDR research projects, at Fenton Hill (US), Rosemanowes (UK) and Hijiori (Japan). This model concentrates on the steady-state flow and heat extraction potentials of the three HDR sites. Bruel (1995) developed a coupled THM FD model of the Rosemanowes (UK) HDR site to investigate connectivity issues involving thermal drawdown in the system.

Advances in computational capabilities, probably linked to rising concerns about climate change further promoted research interest in the field of EGS reservoir modelling after the year 2000. For instance, Ghassemi et al. (2003) developed an integral equation to investigate the effect of heat extraction-induced thermal stress in EGS geothermal reservoirs. Kumar and Ghassemi (2005) developed a numerical model of non-isothermal quartz dissolution in a coupled fracture-matrix EGS system. The model focuses on the effect of thermal stress and silica dissolution on fluid pressure and permeability changes in both the fracture and the rock matrix. Ghassemi and Kumar (2007) later employed the model to investigate the individual and combined effects of chemical and thermal processes on fracture apertures and pressure distribution.

Although many numerical investigations into HDR geothermal reservoirs have now been published, as shown above, the open literature nevertheless reveals a lack of focus on the role of numerical models in predicting the actual responses of EGS reservoirs to thermal stresses. A typical neglected problem is whether tensile stresses predicted in theory are really identified in EGS reservoirs with thermal stress. If we can forecast numerically that the tensile strength of the rock will be exceeded in an EGS reservoir with significant thermal stresses, will the reservoir properties be affected? The objective of the present work is to present some of the ways numerical modelling can be used in the prediction of EGS reservoirs' responses to thermal stresses.

This paper presents a three-dimensional (3D) numerical model of a multifracture EGS reservoir with horizontal wellbores using coupled THM processes. The model is developed and implemented in a single Multiphysics code, COMSOL, with the ability to solve a THM problem directly or indirectly. The direct solution solves the coupling effects employing the available modules provided in the solver; the indirect solution involves using external functions or Livelink simulations to implement the coupled effect. The contribution of this study is threefold. First, the model fully couples the effect of thermal stress to geomechanics, thermal and hydraulic processes, making it more practical than theoretical. Second, the model uses a multifracture system with horizontal wellbores that capture the geomechanical response of each fracture to circulation, instead of a single-fracture system (Ghassemi et al., 2003). Third, the most valuable contribution is the inclusion of a rigorous comparison of all the coupled components of a case with and without thermal stress.

ISSN 2703-4275

2. MATHEMATICAL FORMULATION

Here, the mathematical expressions of the THM model are described. The descriptions include mechanical equilibrium in the rock mass and fractures, the fluid flow conservation in a fully saturated porous medium (with a network of hydraulically conductive fracture systems), and conductive and convective heat transfer in the reservoir. The model is adopted to simulate induced thermal stress due to transient temperature change in EGS reservoirs. The total strain under geomechanical, hydraulic and thermal effects is expressed as:

$$\varepsilon = \left[1/K, 1/H, \alpha_T\right] \cdot \left[\sigma, p, T\right]' \quad (1)$$

where $1/K$, $1/H$ and α_T are the drained compressibility, poroelastic expansion coefficient and volumetric thermal expansion coefficient, respectively. The primary fields are $\sigma, p, and\ T$ (stress, pressure and temperature, respectively). The flow rate is much higher than the bulk deformation; therefore, the quasi-static condition is assumed, and the mass item is ignored. The force equilibrium equation becomes:

$$\left(K + G/3\right)\nabla\left(\nabla \cdot \mathbf{u}\right) + G\nabla^2\mathbf{u} - \alpha\nabla p - K\alpha_T \nabla T = \mathbf{0} \quad (2)$$

where K, G and α are the bulk modulus, shear modulus and Biot coefficient, respectively. For porous fluid flow, the continuity equation is combined with the Darcy's constitutive model, which is expressed as (Aliyu, 2018; Aliyu and Chen, 2017):

$$\frac{\partial \zeta}{\partial t} + \nabla \cdot \left(-\frac{\kappa}{\mu} \nabla p \right) = 0 \quad (3)$$

where ζ, κ and μ are the increment of the fluid volume per unit volume of the bulk, permeability of the porous media and viscosity of the fluid, respectively. The term ζ is affected by changes in the pore pressure, volumetric strain and temperature. It is expressed as:

$$\zeta = \left[\alpha, 1/M, 1/N\right] \cdot \left[\varepsilon, p, T\right]' \quad (4)$$

where $1/M$ and $1/N$ are the normal and analogous constrained specific storage coefficients due to the thermal effect (Zimmerman, 2000; Zimmerman et al., 1993). Substituting (4) into (3) yields:

$$\frac{\partial}{\partial t}\left(\alpha\varepsilon + \frac{1}{M} p + \frac{1}{N} T \right) + \nabla \cdot \left(-\frac{\kappa}{\mu} \nabla p \right) = 0 \quad (5)$$

The coefficient $1/M$ is expressed in terms of porosity ϕ as (Detournay and Cheng, 1993):

$$\frac{1}{M} = \frac{\phi}{K_f} + \frac{\left(\alpha - \phi\right)}{K_s} \quad (6)$$

where K_f is the fluid bulk modulus and K_s is the solid/grain bulk modulus. The coefficient $1/N$ can also be expressed with respect to porosity ϕ as (Detournay and Cheng, 1993):

$$\frac{1}{N} = \alpha_f \phi + \alpha_s \left(\alpha - \phi\right) \quad (7)$$

where α_f is the fluid thermal expansion coefficient and α_s is the solid/grain thermal expansion coefficient. Substituting (6) and (7) into (5) yields:

$$\alpha \frac{\partial\left(\nabla \cdot \mathbf{u}\right)}{\partial t} + \left(\frac{\phi}{K_f} + \frac{\alpha - \phi}{K_s} \right) \frac{\partial p}{\partial t} + \left(\alpha_f \phi + \alpha_s \left(\alpha - \phi\right)\right) \frac{\partial T}{\partial t} - \frac{\kappa}{\mu} \nabla^2 p = 0 \quad (8)$$

The thermal effect contributes to both fluid flow and solid deformation, as illustrated in equations (2) and (8), and the combination of fluid flow and deformation results in heat generation. The equations presented so far assume that fluid flow and deformation processes are rather slow, which could result in negligible heat generation. Thus, a supplementary expression is required for heat transport in porous media. In the fluid, heat transfer is due to convection and conduction, while in the rock matrix, heat transfer is due to conduction. The heat transfer in these two phases is assumed to take place in parallel due to slow seepage. The governing equation for heat transport in porous media is expressed as (Aliyu and Chen, 2016):

$$\left(\rho C\right)_m \frac{\partial T}{\partial t} = -\rho_f C_{p,f} \mathbf{v} \cdot \nabla T + \nabla \cdot \left(\lambda \nabla T\right) \quad (9)$$

where $\left(\rho C\right)_m$ is the sum of heat capacities given as (Aliyu and Chen, 2017):

$$\left(\rho C\right)_m = \left(1 - \phi\right)\left(\rho C\right)_s + \phi\left(\rho C\right)_f \quad (10)$$

The sum of thermal conductivities λ is expressed as:

$$\lambda = \left(1 - \phi\right)\lambda_s + \phi\lambda_f \quad (11)$$

where λ_s and λ_f are the rock thermal conductivity and fluid thermal conductivity, respectively.

In EGS reservoirs, the fracture system is the primary conduit for fluid and heat transport. In this study, the parallel plate concept is adopted to represent the existing fractures which might open after thermal and hydraulic stimulations. The method is commonly used for simulating both tensile and shear failure of rock material (Willis-Richards et al., 1996). For fractures with interlocked joints, Bandis et al. (1983) developed an empirical relationship between effective normal stress σ_n' and deformation, given as (Barton et al., 1985):

$$\sigma_n = \frac{-\Delta V}{\frac{1}{K_{ni}} - \frac{1}{K_{ni} b_{\max}} \Delta V} \quad (12)$$

where σ_n is the normal stress across the fracture, K_{ni} is the initial fracture stiffness, ΔV is the fracture closure due to normal stress, and $b_{\max}$ is the maximum fracture closure. Equating the fracture aperture with the closure and the

Proceedings 42nd New Zealand Geothermal Workshop
24-26 November 2020
Waitangi, New Zealand
ISSN 2703-4275

effective normal stress with the normal stress, the aperture changes can be expressed as:

$$\Delta b = \frac{\Delta \sigma_n'}{K_{ni} - \frac{\Delta \sigma_n'}{b_{\max}}} \quad (13)$$

The denominator of equation (13) represents the fracture stiffness K_n, which increases with the effective normal stress. The stiffness K_n is given as (Barton et al., 1985):

$$K_n = K_{ni}\left(1 - \frac{\sigma_n'}{K_{ni} b_{\max} + \sigma_n'}\right)^{-2} \quad (14)$$

The cubic law provides an expression for the fluid flow in a fracture, where the fracture permeability is described as (Aliyu and Chen, 2018):

$$\kappa_f = \frac{b^2}{12} \quad (15)$$

where b is the fracture aperture or the opening width. The governing equation is given as:

$$\frac{\partial b}{\partial t} - \frac{b^3}{12\mu}\nabla^2 p = -q_l \quad (16)$$

where q_l is the leak-off rate.

3. THM COUPLED FRAMEWORK

The coupled framework of the THM model is formulated in COMSOL Multiphysics using the heat transfer, fluid flow and structural mechanics modules, which provide different means of evaluating the effects of thermal stress and HDR reservoir cooling during injection processes. For example, they permit an evaluation of the physical alterations to the reservoir that emerge from fracture aperture and permeability changes due to large-scale fluid injection/extraction. The complex nature of these changes involves the formation of coupled processes based on a combination of thermal, hydraulic and mechanical laws (Tsang, 1991).

Figure 1 shows the coupled THM framework developed and implemented in the COMSOL Multiphysics solver based on equations (1–16) and other built-in equations available in the solver. The mathematical expressions and functions are derived to approximate thermo-hydro-mechanical processes in COMSOL Multiphysics to evaluate the effects of thermally induced stress in an HDR geothermal reservoir. The solution is achieved using the strain suppression method assuming fixed strain conditions at the boundaries.

The coupling between the fluid flow-deformation (Eq. (1–8)) and the heat transfer (Eq. (9–11)) equations relates to temperature and pressure terms in the force balance equation (Eq. (2)). The dependence of material coefficients (such as strain, stress) on temperature and pore pressure also plays a role. Coupling of permeability and fracture aperture depends on rock deformation, effective stress, stiffness and pore pressure (Eq. (12-16)).

The coupled THM framework equations of fluid flow, heat transport and mechanical balance are solved iteratively in COMSOL to compute the temperature, pressure and displacement fields at each node for each time step. COMSOL Multiphysics uses a Newton iteration that computes the Jacobians automatically to solve nonlinear systems of equations. The software is in-built with numerous iterative solvers for both linear and nonlinear systems, including FGMRES, GMRES, TFQMR, BiCGSTab, and Conjugate gradients. The coupled THM model has previously been validated against experimental measurements of the Fenton Hill HDR reservoir without the thermal stress effect (Aliyu and Archer, 2020a, 2020b, 2020c). To confirm the model's validity here, the thermal stress effect results are compared with those for the case without thermal stress.

4. MODEL DESCRIPTION

Before a numerical model of an EGS geothermal reservoir can be developed, conceptual models and mathematical descriptions of the features and processes of operation are approximated in the form of partial derivatives (McDermott et al., 2005; Tsang, 1999). The level of approximation depends upon the accuracy of the solution obtained and the availability of a computational resource; thus, many simplifying assumptions need to be made (Aliyu et al., 2017, 2016). The key assumptions are described in the following:

- Model development was led by experimental measurements from the HDR reservoir at Fenton Hill, New Mexico (Murphy et al., 1985, 1981);
- The fracture system's geometric configurations in the numerical model were primarily based on direct assumptions of planar fractures;
- The numerical model specifies fractures before any injection process happens; therefore, no new fractures are formed due to circulation processes and reservoir creation.
- Geomechanical changes in the prescribed fracture systems are assumed to be caused by the cold-fluid injection and hot-fluid extraction.

These hypotheses are not perfect but could have relevance for EGS reservoirs.

4.1 Model implementation

Figure 2 presents the geometry of the multifracture EGS reservoir employed. The dimensions of the reservoir are 900 m × 900 m × 900 m. The wellbores have a horizontal length of 750 m with the injection wellbore located at 450 m (y-axis) and -4,400 m (z-axis), and the production well is positioned at 450 m (y-coordinate) and -5,100 m (z-coordinate). A total of seven fractures are implemented in the model with a uniform radius of 400 m each. The fractures are spaced 100 m apart. Physical properties of the reservoir employed in the study comprise: thermal conductivity (2.9 W/m/K), heat capacity (850 J/kg/K), density (2600 kg/m^3), Young's modulus (60 GPa), porosity (0.2), permeability (1e-18 m^2), Biot coefficient (0.79), Biot modulus (1.23e+4 MPa), and solid bulk modulus (50 GPa).

Proceedings 42nd New Zealand Geothermal Workshop
24-26 November 2020
Waitangi, New Zealand
ISSN 2703-4275

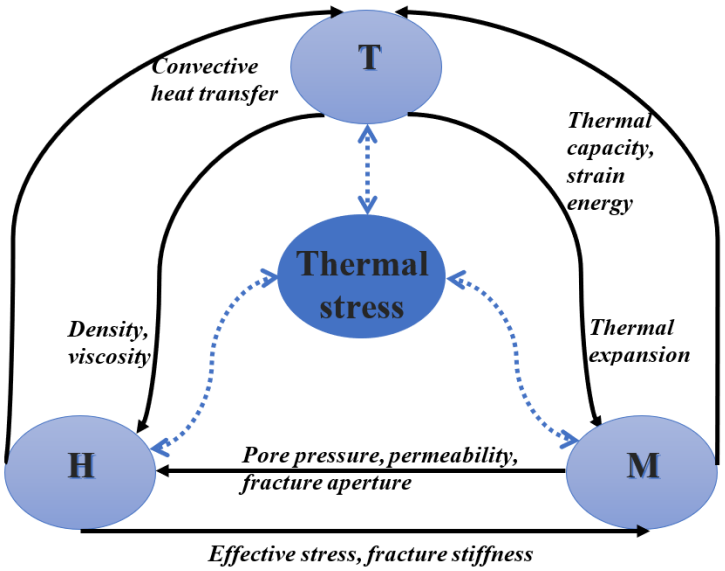

Figure 1: Coupled processes framework

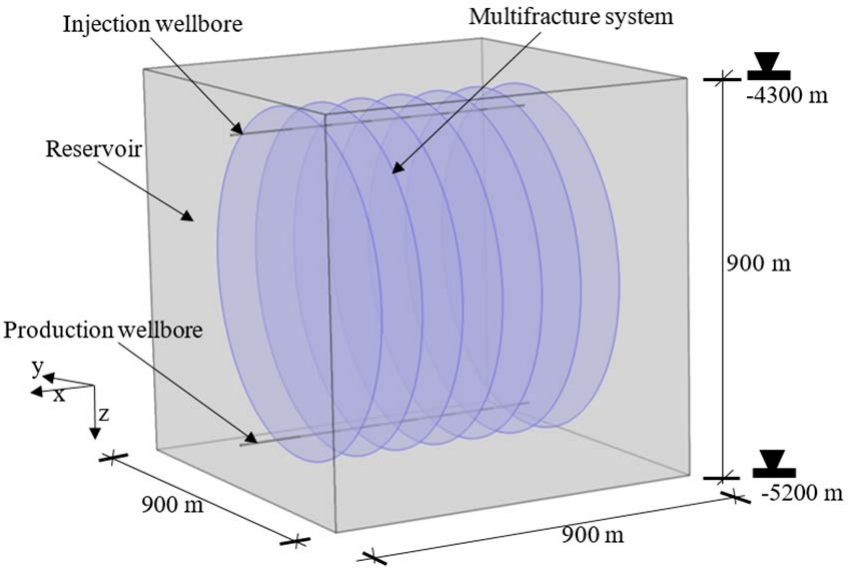

Figure 2: Multifracture HDR reservoir geometry

For the fracture systems the properties used are: thermal conductivity (2.5 W/m/K), heat capacity (900 J/kg/K), density (2000 kg/m^3), Young's modulus (40 GPa), porosity (0.1), initial aperture (0.21 mm), maximum fracture closure (0.02 mm), initial fracture stiffness (1e+5 MPa/m).

4.2 Initial and boundary conditions

The initial stresses for the vertical (σ_v), maximum horizontal (σ_H) and minimum horizontal (σ_h) gradients are 17.31 MPa/km, 15.38 MPa/km and 11.54 MPa/km, respectively. The initial pore pressure is assumed to be hydrostatic.

The initial temperature T_i varies with depth. It is expressed as:

$$T_i = 12°C - 0.06[K/m] \times z \qquad (17)$$

For the thermal boundary conditions, an injection temperature of 40°C is employed at the injection wellbore. The production wellbore is considered as an outlet boundary. All other boundaries are held to be insulated. For the hydraulic boundary conditions, an injection pressure of 20 MPa is applied at the injection wellbore. Likewise, at the production wellbore, a pressure of 2.4 MPa is employed. For the mechanical boundary conditions, a vertical stress of 90 MPa is applied at the top boundary; 80 MPa maximum horizontal stress is employed at the left and right boundaries, and 60 MPa minimum horizontal stress is applied at the front and back boundaries. A roller constraint is employed at all boundaries except at the top of the reservoir.

4. RESULTS

This section analyses nine reservoir parameters based on the implementation of the coupled processes effect. For all the simulation results obtained, a comparative analysis is performed of the scenarios with and without thermal stress.

The coupled processes presented in Figure 1 show a framework for the implementation of the thermal, hydraulic and mechanical interactions encountered in EGS reservoirs with and without thermal stress. In order to justify the implementation and strength of the coupling, this section describes the effects on the basic reservoir parameters.

Figure 3 presents the changes in pore pressure at the production points of the fractures. The curves show the cases with and without thermal stress at a constant injection rate. As can be seen, the pore pressure builds up at the fractures and gradually becomes steady. In all the cases, the pressures are higher with thermal stress because of the thermal shock experienced in the system. The results indicate that thermal stresses enhance the hydraulic fracturing by increasing the initiation and propagation pressures. Furthermore, fluid injection into a fracture with a tiny aperture causes the fracture pressure to rise above the initial reservoir pressure. The pressure build-up is directly proportional to the cold-fluid injection rate. Thus, the thermal stress change can be controlled simply by reducing or increasing the cold-fluid injection temperature.

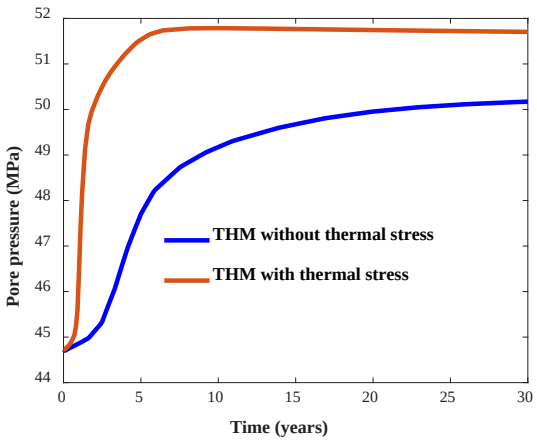

Figure 3: Fracture pore pressure changes at the production points with and without thermal stress

Figure 4 shows the effective stress changes at the production points of the fractures. With thermal stress, the effective stress builds up at the fractures during the first four years due to the thermal shock effect. After seven years, there is a gradual decline in the effective stress until the end of the 30-year simulation. The possible reason for the decrease is because the thermal shock effect has subsided due to the thermal cooling of fractures. Without thermal stress, the effective stress increases gradually as cold-fluid injection continues. The results show that the change in effective stress is more pronounced with thermal stress, which can be attributed to the thermal shock produced by the cold-fluid injection.

Figure 5 presents fracture permeability changes at the production points with and without thermal stress. As seen, for the model with thermal stress, the fracture permeability undergoes a substantial increase as the cold-fluid injection begins. The increase then starts to decline gradually after seven years until the end of the 30-year simulation. The reason for this behaviour is that the hot rock mass has experienced a lower temperature regime that causes it to cool down. The cooling causes the rock to contract with thermal shock as a result of induced thermal stress, which leads to a notable enhancement in the fracture permeability. The decline in the permeability encountered in the later stages is due to a reduction in the thermal stresses caused by the thermal front.

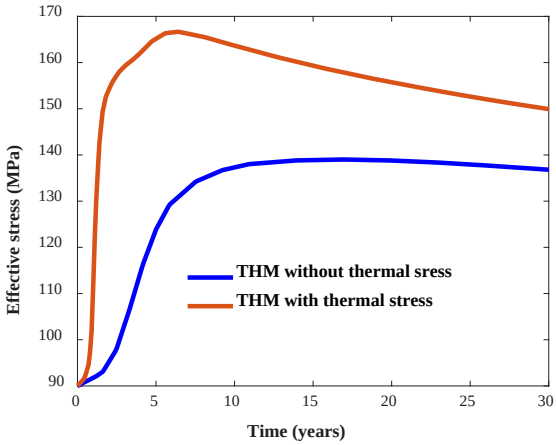

Figure 4: Effective stress changes at the production points with and without thermal stress

For the scenario without thermal stress, the fracture permeability gradually increases during the first two-and-a-half years before a stage of rapid increase is reached. After that, the fracture permeability gradually becomes steady until the end of the 30-year simulation. This is because the fracture permeability changes are only affected by the changes in the pore pressure, stiffness and effective stresses.

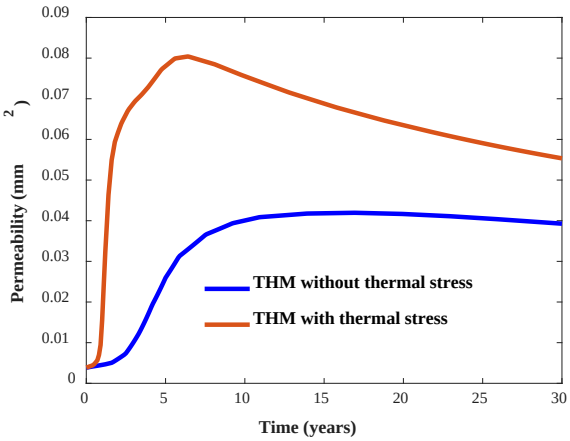

Figure 5: Fracture permeability changes at the production points with and without thermal stress

Figure 6 shows fracture aperture changes at the production points with and without thermal stress. The curves display a similar trend to that shown in Figure 5 due to the direct relationship between the two parameters. The maximum aperture opening with thermal stress is close to 1.0 mm; without thermal stress, it is 0.80 mm. The percentage increments in the apertures with and without thermal stress effect are approximately 388% and 295%, respectively.

Figure 7 presents the fracture stiffness changes at the production points with and without thermal stress. As can be seen, the stiffness is lower with and higher without thermal stress. The reason for this is a substantial strength reduction as the fracture opens due to the fluid injection. The stiffness trend is the opposite of that for fracture permeability and aperture, as shown in Figures 5 and 6.

Proceedings 42nd New Zealand Geothermal Workshop
24-26 November 2020
Waitangi, New Zealand
ISSN 2703-4275

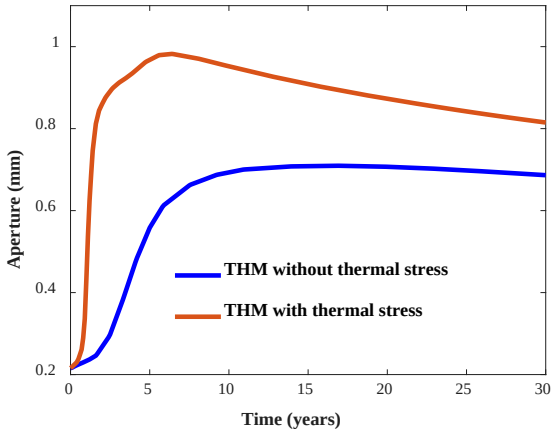

Figure 6: Fracture aperture changes at the production points with and without thermal stress

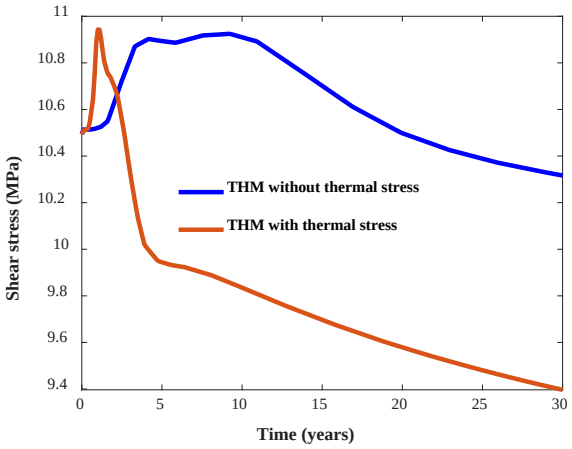

Figure 8: Fracture shear stress changes at the production points with and without thermal stress

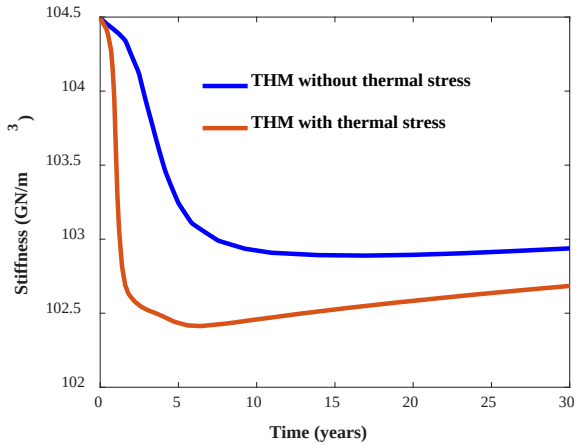

Figure 7: Fracture stiffness changes at the production points with and without thermal stress

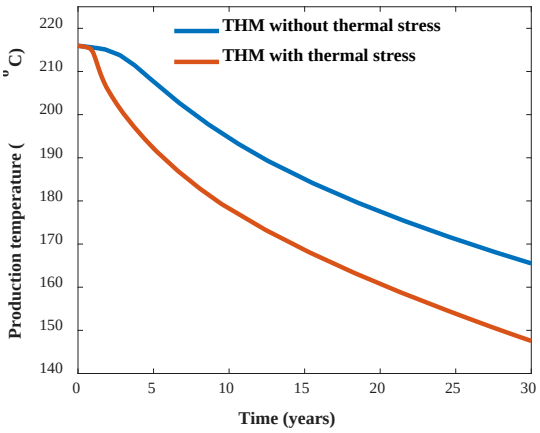

Figure 9: Fracture temperature changes at the production points with and without thermal stress

Figure 8 shows the fracture shear stress changes at the production points with and without thermal stress. The curves show that the fracture shear stresses increase at the early stages of the injection and then decline in the later stages. For the thermal stress case, fracture shear stress builds up from 10.5 MPa to 10.95 MPa during the first two years of injection; after that, the shearing subsides to 9.9 MPa after five years of operation. The shear stress gradually becomes steady for the remaining period of the simulation.

Figure 9 presents the temperature changes at the production wellbore with and without thermal stress. As can be seen, the temperature is lower with and higher without thermal stress. The reason for this is that as the fracture undergoes a substantial thermal front due to the cold-fluid injection, the fracture temperature declines. The temperature trend is the opposite of that for the pore pressure: as the temperature reduces, the pressure increases, as shown in Figures 3.

Figure 10 shows the fluid density changes at the production wellbore with and without thermal stress. The curves show that the fracture fluid densities increase with time in both cases. The fluid density is a temperature-dependent parameter, decreasing with temperature increases and vice versa. In the current case, the temperatures at the production wellbore decrease with time, as shown in Figure 9; this leads to an increase in the densities for both scenarios.

Figure 11 presents the fluid viscosity changes at the production wellbore with and without thermal stress. As can be seen, the fluid viscosity is higher with and lower without thermal stress. With thermal stress, the fluid viscosity increment is more pronounced, indeed almost double that of the case without thermal stress. The reason is that the viscosity entirely depends on the temperature, and the temperature is more affected by thermal stress.

Proceedings 42nd New Zealand Geothermal Workshop
24-26 November 2020
Waitangi, New Zealand
ISSN 2703-4275

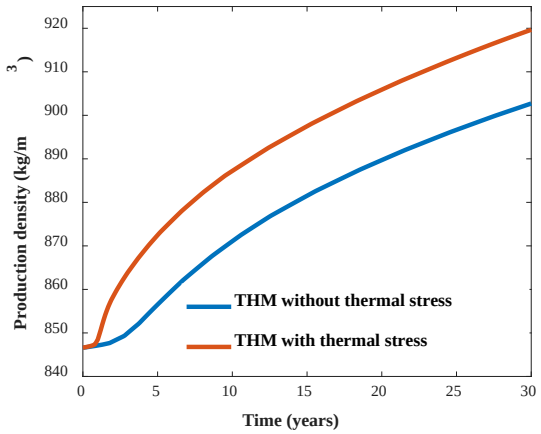

Figure 10: Fluid density changes at the production points with and without thermal stress

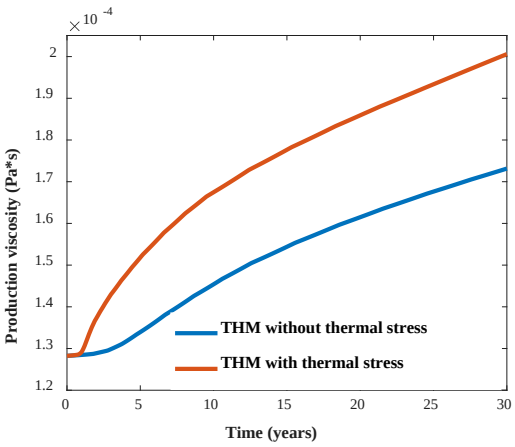

Figure 11: Fluid viscosity changes at the production points with and without thermal stress

6. CONCLUSION

This paper has presented a coupled thermo-hydro-mechanical (THM) model of a multifracture EGS reservoir that accounts for thermal stress effects. The model was used to study the impact of induced thermal stresses on EGS reservoir parameters during cold-fluid injection. Nine reservoir parameters were analysed in-depth to understand the effect of induced thermal stress on reservoir performance. The simulation results were compared with a THM model of the case without thermal stress in order to produce a better judgement of the current model results.

The results show a significant difference between the predictions of the THM models with and without thermal stress related to effects of exploitation on reservoir parameters. For example, when thermal stress is considered, the fracture permeability and aperture increase to a level more than 22.20% above that seen in the case without thermal stress. Fortunately, this can work to the benefit of reservoir productivity, helping to enhance fracture permeability in the near-wellbore region. Based on the simulation work conducted here, it is clear that neglecting the effect of thermal stress in HDR reservoir simulation may result in a miscalculation of the overall output of the reservoir performance.

REFERENCES

Abé, H., Hayashi, K., Arima, S., 1985. Theoretical study on the stability of a reservoir created by the intersection of a fluid-filled crack with an oblique joint for the extraction of geothermal heat. Int. J. Numer. Anal. Methods Geomech. 9, 15–27.

Abé, H., Keer, L.M., Mura, T., 1976a. Growth rate of a penny-shaped crack in hydraulic fracturing of rocks, 2. J. Geophys. Res. 81, 6292–6298.

Abé, H., Keer, L.M., Mura, T., 1979. Theoretical study of hydraulically fractured penny-shaped cracks in hot, dry rocks. Int. J. Numer. Anal. Methods Geomech. 3, 79–96.

Abé, H., Mura, T., Keer, L.M., 1976b. Growth rate of a penny-shaped crack in hydraulic fracturing of rocks. J. Geophys. Res. 81, 5335–5340.

Abé, H., Sekine, H., 1983. Crack-Like Reservoir in Homogeneous and Inhomogeneous HDR. In: Springer. Springer, pp. 447–462.

Al Saedi, A.Q., Flori, R.E., Kabir, C.S., 2019. Exploring alteration of near-wellbore geothermal gradient during fluid circulation and production. J. Pet. Sci. Eng. 177, 909–920.

Aliyu, M.D., 2018. Hot dry rock reservoir modelling. University of Greenwich.

Aliyu, M.D., Archer, R.A., 2020a. Numerical simulation of multifracture HDR geothermal reservoirs. Renew. Energy. Doi: 10.1016/j.renene.2020.09.085

Aliyu, M.D., Archer, R.A., 2020b. Numerical simulation of HDR geothermal energy reservoirs: A thermo-hydro-mechanical model. Geotherm. Resour. Counc. Trans. 44, 1–26.

Aliyu, M.D., Archer, R.A., 2020c. Thermo-hydro-mechanical model of multifracture HDR geothermal reservoirs. Geotherm. Resour. Counc. Trans. 44, 1–28.

Aliyu, M.D., Chen, H.-P., 2017. Optimum control parameters and long-term productivity of geothermal reservoirs using coupled thermo-hydraulic process modelling. Renew. Energy 112.

Aliyu, Musa D., Chen, H.-P., 2017. Sensitivity analysis of deep geothermal reservoir: Effect of reservoir parameters on production temperature. Energy 129, 101–113.

Aliyu, M.D., Chen, H.-P., 2018. Enhanced geothermal system modelling with multiple pore media: Thermo-hydraulic coupled processes. Energy 165, 931–948.

Aliyu, M.D., Chen, H., 2016. Numerical Modelling of Coupled Hydro-Thermal Processes of the Soultz Heterogeneous Geothermal System. In: M. Papadrakakis, V. Papadopoulos, G. Stefanou, V.P. (Ed.), ECCOMAS Congress 2016 VII European Congress on Computational Methods in Applied Sciences and Engineering M. Papadrakakis, V. Papadopoulos, G. Stefanou, V. Plevris (Eds.) Crete

Island, Greece, 5–10 June 2016. Institute of Structural Analysis and Antiseismic Research School of Civil Engineering National Technical University of Athens (NTUA) Greece, Crete Island, Greece, pp. 1659–1671.

Aliyu, Musa D, Chen, H., 2017. Numerical modelling of geothermal reservoirs using the triple porosity-permeability approach. In: Proceedings of the 25th UKACM Conference on Computational Mechanics 12 –13 April 2017, University of Birmingham, Birmingham, United Kingdom. UKACM, Birmingham, pp. 10–13.

Aliyu, M.D., Chen, H., Harireche, O., 2016. Finite element modelling for productivity of geothermal reservoirs via extraction well. In: Proceedings of the 24th UK Conference of the Association for Computational Mechanics in Engineering 31 March– 01 April 2016, Cardiff University, Cardiff. Cardiff, pp. 331–334.

Aliyu, M.D., Chen, H., Harireche, O., Hills, C.D., 2017. Numerical Modelling of Geothermal Reservoirs with Multiple Pore Media. In: PROCEEDINGS, 42nd Workshop on Geothermal Reservoir Engineering Stanford University, Stanford, California, February 13-15, 2017 SGP-TR-212. Stanford, US, pp. 1–12.

Bandis, S.C., Lumsden, A.C., Barton, N.R., 1983. Fundamentals of rock joint deformation. Int. J. Rock Mech. Min. Sci. 20, 249–268.

Barton, N., Bandis, S., Bakhtar, K., 1985. Strength, deformation and conductivity coupling of rock joints. Int. J. Rock Mech. Min. Sci. 22, 121–140.

Bažant, Z.P., Ohtsubo, H., 1978. Geothermal heat extraction by water circulation through a large crack in dry hot rock mass. Int. J. Numer. Anal. Methods Geomech. 2, 317–327.

Bruel, D., 1995. Heat extraction modelling from forced fluid flow through stimulated fractured rock masses: application to the Rosemanowes hot dry rock reservoir. Geothermics 24, 361–374.

Detournay, E., Cheng, A.H.-D., 1993. Fundamentals of Poroelasticity. In: Analysis and Design Methods. Elsevier, pp. 113–171.

Elsworth, D., 1989. Theory of thermal recovery from a spherically stimulated hot dry rock reservoir. J. Geophys. Res. 94, 1927–1934.

Ghassemi, A., Suresh Kumar, G., 2007. Changes in fracture aperture and fluid pressure due to thermal stress and silica dissolution/precipitation induced by heat extraction from subsurface rocks. Geothermics 36, 115–140.

Ghassemi, A., Tarasovs, S., Cheng, A.H.D., 2003. An integral equation solution for three-dimensional heat extraction from planar fracture in hot dry rock. Int. J. Numer. Anal. Methods Geomech. 27, 989–1004.

Harlow, F.H., Pracht, W.E., 1972. A theoretical study of geothermal energy extraction. J. Geophys. Res. 77, 7038–7048.

Hicks, T.W., Pine, R.J., Willis-Richards, J., Xu, S., Jupe, A.J., Rodrigues, N.E.V., 1996. A hydro-thermo-mechanical numerical model for HDR geothermal reservoir evaluation. Int. J. Rock Mech. Min. Sci. Geomech. Abstr. 33, 499–511.

Jupe, A.J., Bruel, D., Hicks, T., Hopkirk, R., Kappelmeyer, O., Kohl, T., Kolditz, O., Rodrigues, N., Smolka, K., Willis-Richards, J., Wallroth, T., Xu, S., 1995. Modelling of a european prototype hdr reservoir. Geothermics 24, 403–419.

Kumar, G.S., Ghassemi, A., 2005. Numerical modeling of non-isothermal quartz dissolution/precipitation in a coupled fracture–matrix system. Geothermics 34, 411–439.

McDermott, C.I., Randriamanjatosoa, A.L., Tenzer, H., Sauter, M., Kolditz, O., 2005. Processes in crystalline HDR geothermal energy recovery: Preliminary application to spa urach. Trans. - Geotherm. Resour. Counc. 29, 649–656.

McFarland, R.D., 1975. Geothermal Reservoir Models--Crack Plane Model, United States Energy Research and Development Administration Contract W-7405-Eng. 36. New Mexico.

Murphy, H., Drake, R., Tester, J., Zyvoloski, G., 1985. Economics of a conceptual 75 MW hot dry rock geothermal electric power-station. Geothermics 14, 459–474.

Murphy, H.D., Tester, J.W., Grigsby, C.O., Potter, R.M., 1981. Energy extraction from fractured geothermal reservoirs in low-permeability crystalline rock. J. Geophys. Res. 86, 7145.

Tsang, C.-F., 1991. Coupled hydromechanical-thermochemical processes in rock fractures. Rev. Geophys. 29, 537.

Tsang, C.-F., 1999. Linking thermal, hydrological, and mechanical processes in fractured rocks. Annu. Rev. Earth Planet. Sci. 27, 359–384.

Willis-Richards, J., Wallroth, T., 1995. Approaches to the modelling of hdr reservoirs: A review. Geothermics 24, 307–332.

Willis-Richards, J., Watanabe, K., Takahashi, H., 1996. Progress toward a stochastic rock mechanics model of engineered geothermal systems. J. Geophys. Res. B Solid Earth 101, 17481–17496.

Zimmerman, R.W., 2000. Coupling in poroelasticity and thermoelasticity. Int. J. Rock Mech. Min. Sci. 37, 79–87.

Zimmerman, R.W., Chen, G., Hadgu, T., Bodvarsson, G.S., 1993. A numerical dual-porosity model with semianalytical treatment of fracture/matrix flow. Water Resour. Res. 29, 2127–2137.